International Journal of Heat and Mass Transfer 52 (2009) 3555–3563

Contents lists available at ScienceDirect

International Journal of Heat and Mass Transfer

journal homepage: www.elsevier.com/locate/ijhmt

Asymmetric wall heat fluxes boundary conditions in double-pass parallel-plate heat exchangers

Chii-Dong Ho *, Wei-Zum Chen, Jr-Wei Tu

Energy and Opto-Electronic Materials Research Center, Department of Chemical and Materials Engineering, Tamkang University, Tamsui, Taipei 251, Taiwan

ARTICLE INFO

Article history:
Received 3 November 2008
Received in revised form 26 February 2009
Accepted 26 February 2009
Available online 17 April 2009

Keywords:
Asymmetric wall heat flux
Parallel-plate device
Double-pass
Conjugated Graetz problems

ABSTRACT

Boundary conditions for asymmetric wall heat fluxes in double-pass parallel-plate laminar countercurrent operations are analyzed theoretically in this work by using an eigenfunction expansion in terms of power series for the homogeneous part and an asymptotic solution for the non-homogeneous part. Effects of variable ratio of heat fluxes on both sides and impermeable-sheet location are also studied. Quantitative and qualitative interpretations of theoretical predictions are utilized to investigate of heat-transfer efficiency enhancement of the double-pass model under consideration as compared to those in the single-pass operations without an impermeable sheet inserted. Results are presented in terms of Nusselt number and device performance improvement. The influence of the impermeable-sheet location on the heat-transfer efficiency enhancement as well as on the power consumption increment in double-pass operations has also been delineated.

1. Introduction

In recent years, the problem of forced convection in a channel between two parallel-plate walls has received considerable attention due to its relevance in connection with cooling of electronic microchannels, heat pipes, nuclear reactors and drying technology. Two different boundary conditions for the thermal response, say constant wall temperature (Dirichlet problem) and constant heat flux (Neumann problem), were presented in a wide variety of heat transfer in engineering applications. The system at steady state with laminar forced convection flow of the negligible axial conduction in cylindrical and parallel-plate geometries is known as the classical Graetz problem [1–2]. Moreover, the more complicated cases of convective heat-transfer problems with non-uniform heating are also investigated by many researchers, such as asymmetric heating [3–5], and periodic heating [6,7].

The surface resistant along the flow path, as expressed in the wall Nusselt number, could be a straightforward manner to analyze the heat-transfer efficiency of multistream or multiphase problems coupling mutual conditions at the interface. The extension of single-stream problems to multistream or multiphase systems, as in conjugated Graetz problems, has been examined by Papoutsakis and Ramkrishna [8,9], Bernier and Baliga [10], Amin and Khan [11] and Yin and Bau [12]. The analytical solution of conjugated Graetz problems is obtained successfully by solving the Sturm–Liouville systems and consequently the solution expressed in the form of the infinite series consisting of the eigenvalue associated with each eigenfunction [13–16], and came out with an infinite number of eigenvalues and only the first negative eigenvalue was used for rapid convergence in the present paper. The alternative configuration with the recycle-effect concept leads to improve the heat-transfer efficiency enhancement due to increasing the fluid velocity but the heat-transfer area as well as the aspect ratio kept unchanged, and applies to many separation processes [17,18] and chemical reactors [19,20].

The present study is an extension of our previous work [21] to apply the case of the asymmetry heating for the conjugated Graetz problem of which the heat fluxes at the walls depending on the ratio of constant heat fluxes q_1'' and q_2'' along each of the walls. The purposes of the present study are to investigate the improvement of device performance, to obtain the wall temperature distribution in the axial direction under variable wall heat fluxes based the superposition technique, and then to discuss the influence of the impermeable-sheet location on the heat-transfer efficiency enhancement with the Graetz number as a parameter as well as on the power consumption increment is also discussed.

2. Temperature distributions in a double-pass heat exchanger

A double-pass heat exchanger is designed by inserting an impermeable sheet into a parallel-plate conduit as shown in Fig. 1. The length and width of the heat exchanger are L and B, respectively. The heights of two subchannels a and b are W_a and W_b, respectively, while the total heat exchanger height is W. Comparing to the device height W, the impermeable sheet thickness δ

* Corresponding author. Tel.: +886 2 26215656; fax: +886 2 26209887.
E-mail address: cdho@mail.tku.edu.tw (C.-D. Ho).

0017-9310/$ - see front matter © 2009 Elsevier Ltd. All rights reserved.
doi:10.1016/j.ijheatmasstransfer.2009.02.038

Nomenclature

a_1	constant defined by Eq. (12)
a_2	integration constants in Eq. (12)
a_3	integration constants in Eq. (12)
B	conduit width, m
b_1	constant defined by Eq. (13)
b_2	integration constants in Eq. (13)
b_3	integration constants in Eq. (13)
D_e	equivalent diameter of the conduit, m
d_{mn}	coefficient in the eigenfunction $F_{a,m}$
e_{mn}	coefficient in the eigenfunction $F_{b,m}$
F_m	eigenfunction associated with eigenvalue λ_m
f	friction factor
G_m	function defined during the use of orthogonal expansion method
Gz	Graetz Number, $VW/\alpha BL$
$\overline{h}$	average heat-transfer coefficient kW/m K
I_h	heat-transfer enhancement, defined by Eq. (43)
I_p	power consumption increment of, defined by Eq. (44)
k	thermal conductivity of the fluid, W/m K
L	conduit length, m
ℓw_f	friction loss in conduit, N m/kg
m	numbers of eigenvalues
$\overline{Nu}$	average Nusselt number
n	terms of power series
P	power consumption, N m/s
Q_r	wall heat flux ratio, $q_2''/(q_1''+q_2'')$
q_1''	heat flux on the down wall, J/m^{2}s
q_2''	heat flux on the upper wall, J/m^{2}s
Re	Reynolds number
S_m	expansion coefficient associated with eigenvalue λ_m
T	temperature, K
V	fluid volume flow rate, m^3/s
v	velocity distribution of fluid, m/s
$\overline{v}$	average velocity of fluid, m/s
W	conduit height, m
x	transversal coordinate, m
z	longitudinal coordinate, m

Greek symbols

α	thermal diffusivity of fluid, m^2/s
Δ	impermeable sheet location, W_a/W
δ	impermeable sheet thickness, m
η	transversal coordinate, x/W
θ	defined by Eqs. (4) and (5)
λ_m	eigenvalue
μ	fluid viscosity, kg/ms
ξ	longitudinal coordinate, $z/(LGz)$
ρ	fluid density, kg/m^3
ϕ	defined by Eqs. (4) and (5)
ψ	dimensionless temperature, $2k(T-T_i)/(q_1''+q_2'')W$
$\overline{\psi}$	dimensionless bulk temperature

Subscripts

a	subchannel a
b	subchannel b
F	at the outlet
i	at the inlet
L	at the end of the channel
0	in a single-pass device
s	at the wall surface

can be neglected, say $\delta << W$. The fluid with volumetric flow rate V and temperature T_i firstly feeds into the subchannel a and then, the fluid was pumped into subchannel b at the conduit end with the aid of a convectional pump. The fluid was heated by the down and upper walls with constant heat fluxes q_1'' and q_2''.

To simply the mathematical statement, the following assumptions are made: (1) the physical properties of fluid are constant; (2) the fluid is fully-developed laminar flow in each channel; (3) the entrance length and end effects are neglected; (4) the longitudinal heat conduction is ignored comparing to the longitudinal heat convection; (5) the fluid is well-mixed at the inlet and the outlet of each subchannel; (6) the thermal resistance of inserting impermeable sheet can be neglected. Based on these assumptions, the energy balance equations and the velocity distributions of a double-pass heat exchanger with asymmetry wall heat fluxes are formulated and are the same as the previous work [21] except the boundary conditions on the walls as follows:

$$\frac{\partial \psi_a(0,\xi)}{\partial \eta_a} = -2Q_r\Delta \tag{1}$$

$$\frac{\partial \psi_b(0,\xi)}{\partial \eta_b} = -2(1-Q_r)(1-\Delta) \tag{2}$$

The dimensionless groups in the Eqs. (1), (2) are

$$\eta_a = \frac{x_a}{W_a},\quad \eta_b = \frac{x_b}{W_b},\quad \xi = \frac{z}{LGz},\quad \psi_a = \frac{2k(T_a-T_i)}{(q_1''+q_2'')W},$$
$$\psi_b = \frac{2k(T_b-T_i)}{(q_1''+q_2'')W},\qquad \Delta = \frac{W_a}{W},\quad Q_r = \frac{q_1''}{q_1''+q_2''},\quad Gz = \frac{VW}{\alpha BL} \tag{3}$$

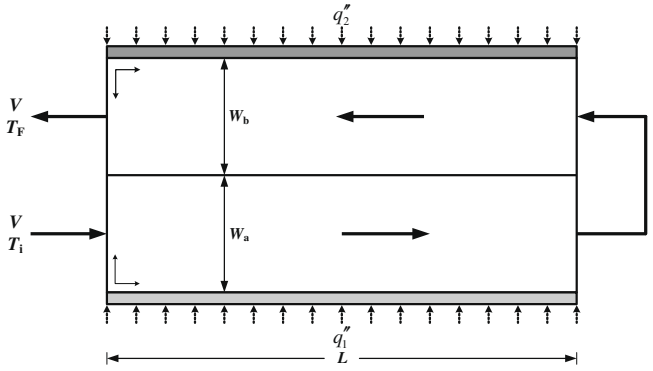

Fig. 1. Double-pass parallel-plate heat exchanger.

According to our previous study [21], the inhomogeneous boundary conditions (Eqs. (1) and (2)) can be removed by the linear superposition of an asymptotic solution, $\theta(\eta,\xi)$, and a homogeneous solution, $\varphi(\eta,\xi)$, and the complete solutions are as follows:

$$\psi_a(\eta_a,\xi) = \theta_a(\eta_a,\xi) + \phi_a(\eta_a,\xi) \tag{4}$$

$$\psi_b(\eta_b,\xi) = \theta_b(\eta_b,\xi) + \phi_b(\eta_b,\xi) \tag{5}$$

2.1. Asymptotic solution of inhomogeneous boundary conditions

Substituting Eqs. (4) and (5) into energy balance equations, the governing equations with inhomogeneous boundary conditions can be written as

$$\frac{\partial^2\theta_a(\eta_a,\xi)}{\partial\eta_a^2}=\left[(6\eta_a-6\eta_a^2)\frac{(\Delta W)^2}{\alpha LGz}\right]\frac{\partial\theta_a(\eta_a,\xi)}{\partial\xi} \tag{6}$$

$$\frac{\partial^2\theta_b(\eta_b,\xi)}{\partial\eta_b^2}=\left[(6\eta_a-6\eta_a^2)\frac{(1-\Delta)^2W^2}{\alpha LGz}\right]\frac{\partial\theta_b(\eta_b,\xi)}{\partial\xi} \tag{7}$$

$$\frac{\partial\theta_a(0,\xi)}{\partial\eta_a}=-2Q_r\Delta \tag{8}$$

$$\frac{\partial\theta_b(0,\xi)}{\partial\eta_b}=-2(1-Q_r)(1-\Delta) \tag{9}$$

$$\theta_a(1,\xi)=\theta_b(1,\xi) \tag{10}$$

$$\frac{\partial\theta_a(1,\xi)}{\partial\eta_a}=-\frac{\Delta}{1-\Delta}\frac{\partial\theta_b(1,\xi)}{\partial\eta_b} \tag{11}$$

As reported in the previous study [3,21], while the fluid temperature profile reaches the thermal fully-developed under the constant heat fluxes on the walls, the fluid temperature profile is unchanged in the radial direction and increased linear in ξ. Therefore, the asymptotic solutions of $\theta_a(\eta_a,\xi)$ and $\theta_b(\eta_b,\xi)$ can be taken as following forms

$$\theta_a(\eta_a,\xi)=a_1\xi+a_1\Delta\left(\eta_a^3-\frac{1}{2}\eta_a^4\right)+a_2\eta_a+a_3 \tag{12}$$

$$\theta_b(\eta_b,\xi)=b_1\left(\frac{1}{Gz}-\xi\right)+b_1(1-\Delta)\left(\eta_b^3-\frac{1}{2}\eta_b^4\right)+b_2\eta_b+b_3 \tag{13}$$

in which a_1 and b_1 are the undetermined constants and a_2, a_3, b_2 and b_3 are the integration constants. Substituting Eqs. (12) and (13) into the boundary conditions Eqs. (8) and (9) gives

$$a_2=-2Q_r\Delta \tag{14}$$

$$b_2=-2(1-Q_r)(1-\Delta) \tag{15}$$

2.2. Eigenfunction expansions of the homogeneous problem

The homogeneous problem for the functions $\varphi_a(\eta_a,\xi)$ and $\varphi_b(\eta_b,\xi)$ is the same as that reported in previous work [21]. Hence, the analytical solutions of the homogeneous problem are in the form

$$\phi_a(\eta_a,\xi)=\sum_{m=0}^{\infty}S_{a,m}F_{a,m}(\eta_a)G_m(\xi) \tag{16}$$

$$\phi_b(\eta_b,\xi)=\sum_{m=0}^{\infty}S_{b,m}F_{b,m}(\eta_b)G_m(\xi) \tag{17}$$

where

$$G_m(\xi)=e^{-\lambda_m\left(\frac{1}{Gz}-\xi\right)} \tag{18}$$

$$F_{a,m}(\eta)=\sum_{n=0}^{\infty}d_{mn}\eta^n,\quad d_{m0}=1(\text{selected}),\quad d_{m1}=0 \tag{19}$$

$$F_{b,m}(\eta)=\sum_{n=0}^{\infty}e_{mn}\eta^n,\quad e_{m0}=1(\text{selected}),\quad e_{m1}=0 \tag{20}$$

2.3. Complete solution of a double-pass parallel-plate heat exchanger

To obtain the complete solution of a double-pass parallel-plate heat exchanger with asymmetric wall heat fluxes, one should firstly determine the six unknowns, say a_1, a_3 b_1 and b_3 for inhomogeneous part and $S_{a,m}$ and $S_{b,m}$ in homogeneous part. These six unknowns can be solved by using the boundary conditions and the orthogonality conditions, average dimensionless inlet temperature, average dimensionless outlet temperature, and the well-mixed temperature at both subchannel ends, as follows. According to our previous work [21], one can get the orthogonality conditions when $n\neq m$:

$$W_b\int_0^1\left[\frac{W_a^2v_a(\eta_a)}{\alpha LGz}\right]S_{a,m}S_{a,n}F_{a,m}F_{a,n}d\eta_a+W_a\int_0^1\left[\frac{W_b^2v_b(\eta_b)}{\alpha LGz}\right]S_{b,m}S_{b,n}F_{b,m}F_{b,n}d\eta_b=0 \tag{21}$$

When $n=m$, one can obtain

$$\begin{aligned}&W_b\int_0^1\frac{W_a^2v_a}{\alpha GzL}S_{a,m}^2F_{a,m}^2(\eta_a)e^{-\frac{\lambda_m}{Gz}}d\eta_a+W_a\int_0^1\frac{W_b^2v_b}{\alpha GzL}S_{b,m}^2F_{b,m}^2(\eta_b)e^{-\frac{\lambda_m}{Gz}}d\eta_b\\&=W_b\int_0^1\frac{W_a^2v_a}{\alpha GzL}\left(-a_1\Delta\left(\eta_a^3-\frac{1}{2}\eta_a^4\right)-a_2\eta_a-a_3\right)S_{a,m}F_{a,m}(\eta_a)d\eta_a\\&\quad+W_a\int_0^1\frac{W_b^2v_b}{\alpha GzL}\left(\frac{2}{Gz}-b_1(1-\Delta)\left(\eta_b^3-\frac{1}{2}\eta_b^4\right)-b_2\eta_b-b_3\right)\\&\quad\times S_{b,m}F_{b,m}(\eta_b)d\eta_b\end{aligned} \tag{22}$$

or

$$\begin{aligned}&W_bS_{a,m}^2e^{-\frac{\lambda_m}{Gz}}\left[F_{a,m}(1)\frac{\partial F'_{a,m}(1)}{\partial\lambda_m}-F_{a,m}(0)\frac{\partial F'_{a,m}(0)}{\partial\lambda_m}-F'_{a,m}(1)\frac{\partial F_{a,m}(1)}{\partial\lambda_m}\right]\\&\quad+W_aS_{b,m}^2e^{-\frac{\lambda_m}{Gz}}\left[F_{b,m}(1)\frac{\partial F'_{b,m}(1)}{\partial\lambda_m}-F_{b,m}(0)\frac{\partial F'_{b,m}(0)}{\partial\lambda_m}-F'_{b,m}(1)\frac{\partial F_{b,m}(1)}{\partial\lambda_m}\right]\\&=W_b\int_0^1\frac{W_a^2v_a}{\alpha GzL}\left(-a_1\Delta\left(\eta_a^3-\frac{1}{2}\eta_a^4\right)-a_2\eta_a-a_3\right)S_{a,m}F_{a,m}(\eta_a)d\eta_a\\&\quad+W_a\int_0^1\frac{W_b^2v_b}{\alpha GzL}\left(\frac{2}{Gz}-b_1(1-\Delta)\left(\eta_b^3-\frac{1}{2}\eta_b^4\right)-b_2\eta_b-b_3\right)S_{b,m}F_{b,m}(\eta_b)d\eta_b\end{aligned} \tag{23}$$

The average dimensionless inlet temperature $\overline{\psi}_{a,i}$ may be calculated at the inlet of subchannel a by

$$\begin{aligned}\overline{\psi}_{a,i}&=\frac{\int_0^1v_a(\eta_a)BW_a\psi_a(\eta_a,0)d\eta_a}{V}\\&=\int_0^1(6\eta_a-6\eta_a^2)\left[a_1\Delta\left(\eta_a^3-\frac{1}{2}\eta_a^4\right)-2Q_r\Delta\eta_a+a_3\right]d\eta_a\\&\quad+\frac{1}{\Delta}\sum_{m=0}^{\infty}\frac{e^{-\frac{\lambda_m}{Gz}}S_{a,m}}{\lambda_m}\{F'_{a,m}(1)-F'_{a,m}(0)\}=0\end{aligned} \tag{24}$$

The average dimensionless outlet temperature $\overline{\psi}_F$ can be determined by

$$\begin{aligned}\overline{\psi}_F&=-\frac{\int_0^1v_b(\eta_b)BW_b\psi_b(\eta_b,0)d\eta_b}{V}\\&=\int_0^1(6\eta_b-6\eta_b^2)\left[\frac{b_1}{Gz}+b_1(1-\Delta)\left(\eta_b^3-\frac{1}{2}\eta_b^4\right)-2(1-Q_r)(1-\Delta)\eta_b+b_3\right]d\eta_b\\&\quad-\left(\frac{1}{1-\Delta}\right)\sum_{m=0}^{\infty}\frac{e^{-\frac{\lambda_m}{Gz}}S_{b,m}}{\lambda_m}\{F'_{b,m}(1)-F'_{b,m}(0)\}=\frac{2}{Gz}\end{aligned} \tag{25}$$

Furthermore, due to the fluid is well-mixed at the inlet and outlet of each channel, the two subchannel average temperatures at the ends of conduit are the same, as shown in Eq. (26) or Eq. (27)

$$\begin{aligned}\overline{\psi}_{aL}=\overline{\psi}_{bL}&=\int_0^1\frac{v_a(\eta_a)W_aB}{V}\psi_a\left(\eta_a,\frac{1}{Gz}\right)d\eta_a\\&=-\int_0^1\frac{v_b(\eta_b)W_bB}{V}\psi_b\left(\eta_b,\frac{1}{Gz}\right)d\eta_b\end{aligned} \tag{26}$$

or

$$\begin{aligned}&\int_0^1(6\eta_a-6\eta_a^2)\left[\frac{a_1}{Gz}+a_1\Delta\left(\eta_a^3-\frac{1}{2}\eta_a^4\right)-2Q_r\Delta\eta_a+a_3\right]d\eta_a\\&\quad+\frac{1}{\Delta}\sum_{m=0}^{\infty}\frac{S_{a,m}}{\lambda_m}\{F'_{a,m}(1)-F'_{a,m}(0)\}\\&=\int_0^1(6\eta_b-6\eta_b^2)\left[b_1(1-\Delta)\left(\eta_b^3-\frac{1}{2}\eta_b^4\right)-2(1-Q_r)(1-\Delta)\eta_b+b_3\right]d\eta_b\\&\quad-\frac{1}{1-\Delta}\sum_{m=0}^{\infty}\frac{S_{b,m}}{\lambda_m}\{F'_{b,m}(1)-F'_{b,m}(0)\}\end{aligned} \tag{27}$$

Once all the undetermined constants in Eqs. (12), (13) and coefficients in (16), (17) are obtained, the dimensionless temperature distributions of both subchannels are thus obtained in terms of

the Graetz number (Gz), eigenvalues (λ_m), expansion coefficients ($S_{a,m}$ and $S_{b,m}$), impermeable-sheet location (Δ) and associated eigenfunctions ($F_{a,m}(\eta_a)$ and $F_{b,m}(\eta_b)$).

3. Temperature distributions in a single-pass device

The single-pass device of the same working dimensions without impermeable sheet inserting is shown in Fig. 2. The governing equation and velocity distribution may be written as

$$\frac{\partial^2\psi_0(\eta,\xi)}{\partial\eta^2}=\left[\frac{v_0(\eta)W^2}{\alpha GzL}\right]\frac{\partial\psi_0(\eta,\xi)}{\partial\xi} \tag{28}$$

and

$$v_0(\eta)=\frac{V}{WB}(6\eta-6\eta^2) \tag{29}$$

The boundary condition and initial conditions for solving Eq. (28) are

$$\frac{\partial\psi_0(0,\xi)}{\partial\eta}=-2Q_r \tag{30}$$

$$\frac{\partial\psi_0(1,\xi)}{\partial\eta}=2(1-Q_r) \tag{31}$$

$$\psi_0(\eta,0)=0 \tag{32}$$

The calculation procedure is similar to that present in Section 2. The complete solution of single-pass heat exchanger is

$$\psi_0(\eta,\xi)=\theta_0(\eta,\xi)+\phi_0(\eta,\xi) \tag{33}$$

where

$$\theta_0=2\xi-2Q_r\eta+2\eta^3-\eta^4+Q_r-\frac{9}{35} \tag{34}$$

$$\phi_0(\eta,\xi)=\sum_{m=0}^{\infty}S_{0,m}F_{0,m}(\eta)G_{0,m}(\xi) \tag{35}$$

The constants in Eq. (34) are solved by the boundary conditions and the energy balance equation. The $S_{0,m}$ is determined by the initial condition

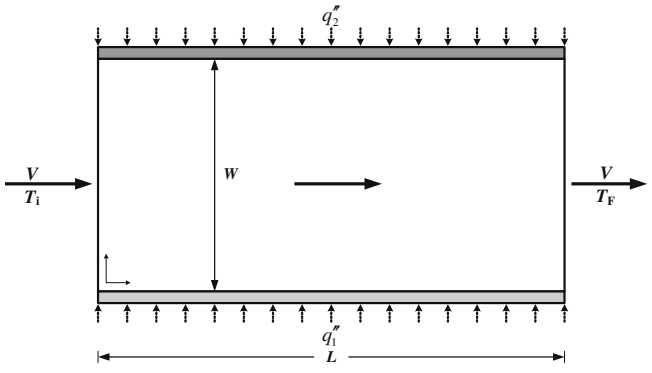

Fig. 2. Single-pass parallel-plate heat exchanger.

$$S_{0,m}=\frac{\int_0^1\left(\frac{v_0(\eta)W^2}{\alpha GzL}\right)[2Q_r\eta-2\eta^3+\eta^4-Q_r+\frac{9}{35}]F_{0,m}(\eta)d\eta}{\int_0^1\left(\frac{v_0(\eta)W^2}{\alpha GzL}\right)e^{-\frac{\lambda_m}{Gz}}[F_{0,m}(\eta)]^2d\eta} \tag{36}$$

4. Heat-transfer efficiency enhancement

In force convection heat-transfer problem, Nusselt number usually uses to measure the convection heat transfer occurring at the wall surface [22]. The average Nusselt number for double-pass operation with a negligible thermal resistance sheet inserting is defined as

$$\overline{Nu}=\frac{\overline{h}W}{k} \tag{37}$$

The average heat-transfer coefficient $\overline{h}$ is determined by making the energy balance around the whole system

$$\overline{h}(2BL)\left(\overline{T}_s-\frac{T_i+T_F}{2}\right)=\rho C_pV(T_F-T_i) \tag{38}$$

or

$$\overline{h}=\frac{\rho C_pV}{BL}\frac{T_F-T_i}{[2(\overline{T}_s-T_i)-(T_F-T_i)]}=\frac{\rho C_pV}{BL}\frac{\psi_F}{(2\overline{\psi}_s-\psi_F)} \tag{39}$$

where

$$\overline{T}_s=\frac{\overline{T}_{as}+\overline{T}_{bs}}{2}=\frac{\int_0^L T_a(0,z)dz+\int_0^L T_b(0,z)dz}{2} \tag{40}$$

Substituting Eq. (39) into Eq. (37) gives

$$\overline{Nu}=\frac{\overline{h}W}{k}=\frac{VW}{\alpha BL}\frac{\psi_F}{(2\overline{\psi}_s-\psi_F)}=\frac{Gz}{Gz\overline{\psi}_s-1} \tag{41}$$

Similarly, for the single-pass operation, the definition of average Nusselt number is

$$\overline{Nu}_0=\frac{Gz}{Gz\overline{\psi}_{s,0}-1} \tag{42}$$

The heat-transfer efficiency enhancement by employing a double-pass device with a negligible thermal resistance sheet inserting is defined by the percentage increase in heat transfer rate based on that in a single-pass device

$$I_h=\frac{\overline{Nu}-\overline{Nu}_0}{\overline{Nu}_0}=\frac{Gz\overline{\psi}_{s,0}-1}{Gz\overline{\psi}_s-1}-1 \tag{43}$$

where the heat-transfer efficiency enhancement is calculated based on the same working dimensions and operating parameters.

5. Power consumption increment

The power consumption of fluid flowing through a device may be determined by friction losses caused by a joint, a diversion, a

Table 1
Convergence of power series in Eqs. (39) and (40) for $n = 30$ and 35 with $\Delta = 0.5$ and $Q_r = 0.7$.

Gz	n	λ_m	$S_{a,m}$	$S_{b,m}$	a_1	a_3	b_1	b_3	$\overline{Nu}$
1	30	−2.18	2.20×10^{-16}	2.45×10^{-18}	4.23	0.08	−2.23	0.08	0.36
	35	−2.18	3.74×10^{-16}	-5.38×10^{-18}	4.23	0.08	−2.23	0.08	0.36
10	30	−2.18	-4.55×10^{-16}	-1.22×10^{-16}	1.81	0.23	0.19	0.23	3.07
	35	−2.18	-5.69×10^{-16}	-1.08×10^{-16}	1.81	0.23	0.19	0.23	3.07
100	30	−2.18	8.35×10^{-16}	1.72×10^{-16}	1.57	0.25	0.44	0.25	5.04
	35	−2.18	-1.40×10^{-16}	-2.50×10^{-17}	1.57	0.25	0.4	0.25	5.04
1000	30	−2.18	-2.68×10^{-14}	-5.57×10^{-15}	1.54	0.25	0.46	0.25	5.35
	35	−2.18	-2.00×10^{-14}	-4.15×10^{-15}	1.54	0.25	0.46	0.25	5.35

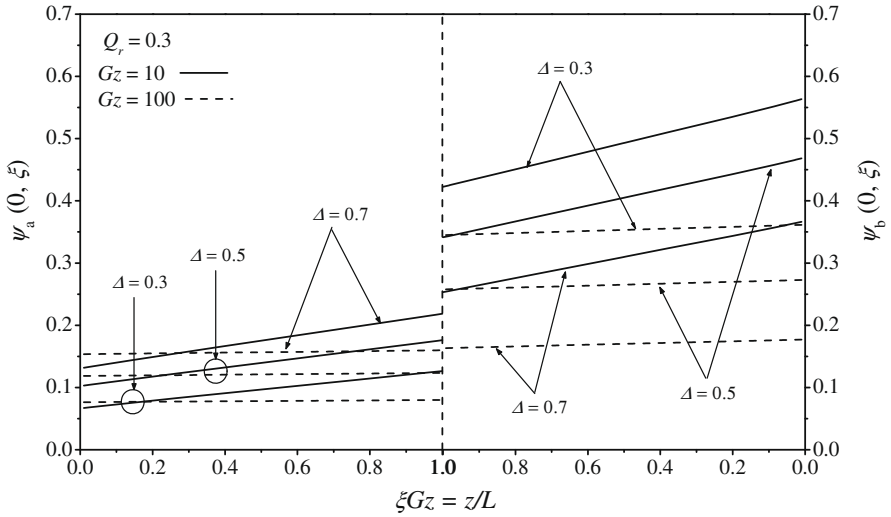

Fig. 3. Dimensionless wall temperature distribution with Δ and Gz as parameters; $Q_r = 0.3$.

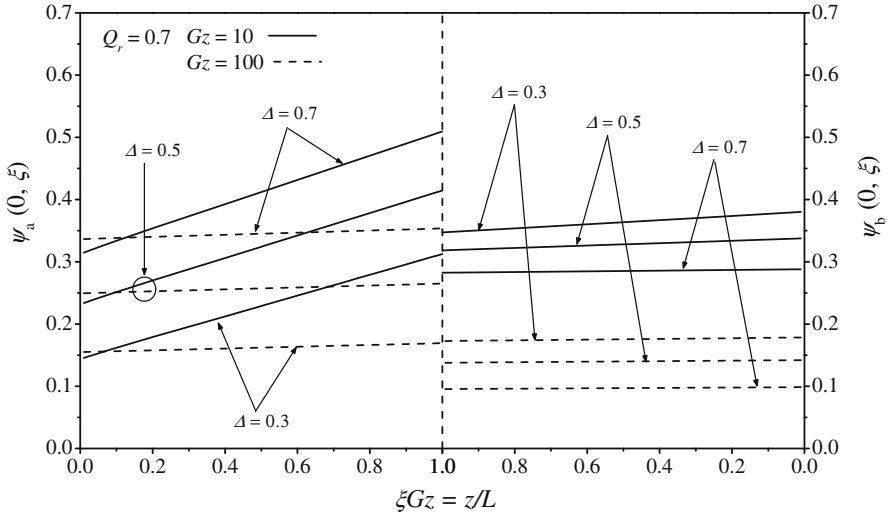

Fig. 4. Dimensionless wall temperature distribution with Δ and Gz as parameters; $Q_r = 0.7$.

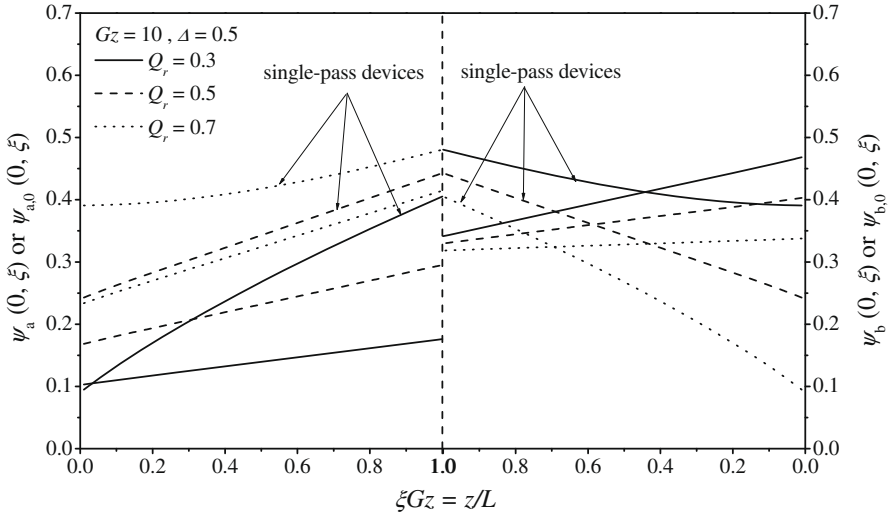

Fig. 5. Comparison of dimensionless wall temperature distributions $\psi(0,\xi)$ and $\psi_0(0, \xi)$ with Q_r as a parameter; $\Delta = 0.5$ and $Gz = 10$.

bending of a tube or the conduit wall. For simplicity to make comparison, only the wall friction loss is considered in calculating the power consumption increment of double-pass operations in the present study. The power consumption increment, I_p, of a double-pass device is defined based on the power consumption in a single-pass device as reported in previous work [21] as follows:

$$I_p = \frac{P - P_0}{P_0} = \frac{V\rho[\ell w_{f,a} + \ell w_{f,b}] - V\rho\ell w_{f,0}}{V\rho\ell w_{f,0}} = \frac{1}{\Delta^3} + \frac{1}{(1-\Delta^3)} - 1 \tag{44}$$

6. Results and discussions

6.1. Temperature distribution in a double-pass device

The energy balances of a double-pass parallel-plate heat exchanger under asymmetric wall heat fluxes were solved with the aid of the linear superposition of the asymptotic solutions, Eqs. (12) and (13), and homogeneous solutions, Eqs. (16) and (17). As referred to Table 1, the convergence of the power series of Eqs. (19) and (20) is $n = 30$ while the two finite series of $n = 30$ and 35 agree reasonably well for the power series due to the resulting average Nusselt numbers are the same for the cases for $\Delta = 0.5$ and $Q_r = 0.7$.

The dimensionless wall temperature distributions with Δ and Gz as parameters for $Q_r = 0.3$ and 0.7 are shown in Figs. 3 and 4, respectively. As shown in Figs. 3 and 4, the wall temperature distributions are linear on the bottom and upper walls and increase with the fluid flowing direction. According to the definition of Q_r in Eq. (3), $Q_r < 0.5$ refers that the heat flux is higher on bottom wall than that on upper wall, while $Q_r > 0.5$ is inverse and $Q_r = 0.5$ is the symmetric heating case. Therefore, for $Q_r = 0.3$, the temperature on bottom wall is always lower than upper wall, as shown in Fig. 3. However, for $Q_r = 0.7$, in order to keep higher heat fluxes on bottom walls, the bottom wall temperature may higher than upper wall temperature, as shown in Fig. 4. Therefore, although the average fluid temperature are the same at $z/L = 1$ in both subchannels, the bottom and upper wall temperatures are different at $z/L = 1$ due to the different wall heat fluxes on the bottom and upper walls for the cases of $Q_r = 0.3$ and $Q_r = 0.7$, and thus, the temperature jump occurs at $z/L = 1$, as shown in Figs. 3 and 4. The heights of subchannels a and b are adjusted by the impermeable-sheet location Δ. As defined in Eq. (3), the height of subschannel a increases with increasing Δ and the height of subschannel b consequently decreases. The influences of impermeable-sheet location Δ on the dimensionless wall temperature distributions are also illustrated in Figs. 3 and 4. Due to the average fluid velocity in subschannel a decreases with increasing the height of subschannel a under constant flow rate V, both the residual time of fluid in subschannel a and the average fluid temperature increase with increasing Δ. Therefore, in order to maintain the constant wall heat fluxes, the bottom wall temperature increases with increasing Δ, as demonstrated in Figs. 3 and 4. On the contrary, the upper wall temperature decreases with increasing Δ. The larger Graetz number Gz represents the higher volumetric flow rate or shorter conduit length resulting in shorter fluid residence time and lower dimensionless outlet temperature, as confirmed by Eq. (25). Hence, the dimensionless wall temperature varies more flatly along the axial direction for $Gz = 100$ than that for $Gz = 10$, as illustrated in Figs. 3 and 4. The dimensionless wall temperature comparison of double-pass devices and single-pass devices is shown in Fig. 5. Two results are concluded by observing from Fig. 5 under the fixed impermeable-sheet location $\Delta = 0.5$ condition: (1) the down wall temperature increases with Q_r and contrarily, the upper wall temperature decreases with Q_r, as illustrated in Fig. 5; (2) comparing to single-pass operation, the double-pass may performs lower wall temperature especially for lower Q_r. In double-pass devices, the fluid in subchannel a is not only heated by the wall but also by the fluid in the subchannel b through the impermeable sheet due to the temperature difference between subchannels a and b. Therefore, the average fluid temperature of subchannel a may be higher than that in single-pass devices, especially at the region near conduit inlet and small Q_r. Accordingly, the bottom wall temperature of double-pass devices at low z/L is higher than that in single-pass devices for the case of $Q_r = 0.3$, as shown in Fig. 5. Fig. 6(a) and (b) illustrate the bottom and upper wall temperatures at the initial point ($\xi Gz = 0$), midpoint ($\xi Gz = 0.5$) and endpoint ($\xi Gz = 1$), respectively, with Δ and Q_r as parameters for $Gz = 100$. The bottom wall temperatures at initial point, midpoint and endpoint increase with increasing Δ and Q_r as shown in Fig. 6(a). However, for the upper wall, the trends of the wall temperatures at initial point, midpoint and endpoint to the Δ and Q_r are inversely compared to the bottom

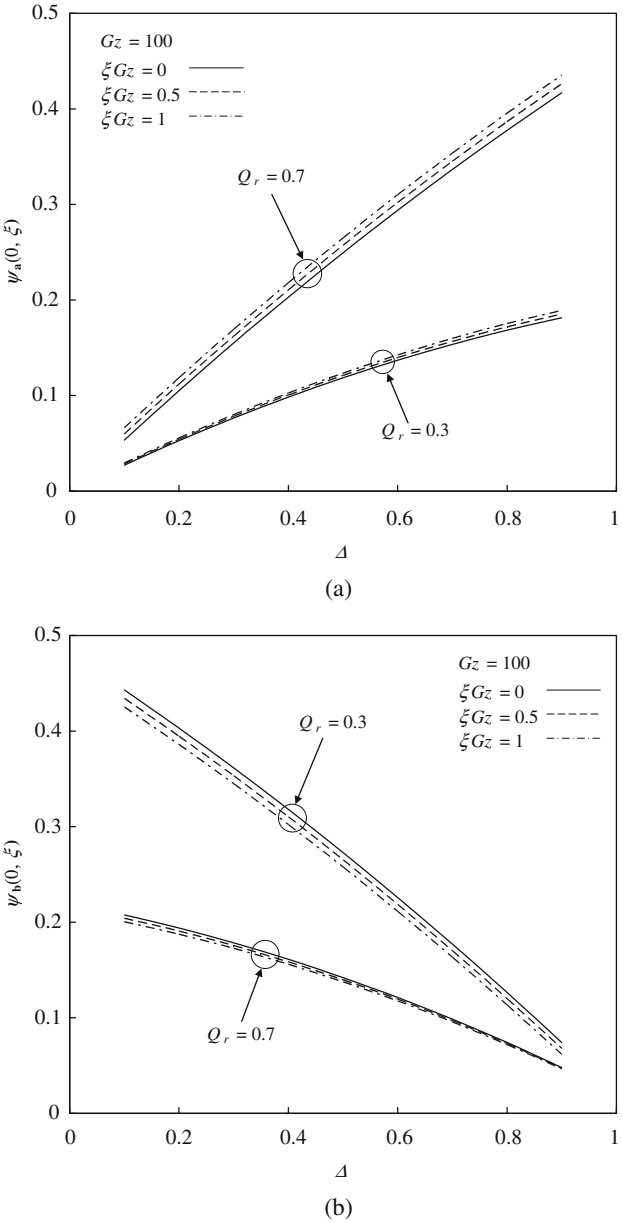

Fig. 6. Initial point ($\xi Gz = 0$), midpoint ($\xi Gz = 0.5$) and endpoint ($\xi Gz = 1$) wall temperatures with Δ and Q_r as parameters for $Gz = 100$, (a) bottom wall and (b) upper wall.

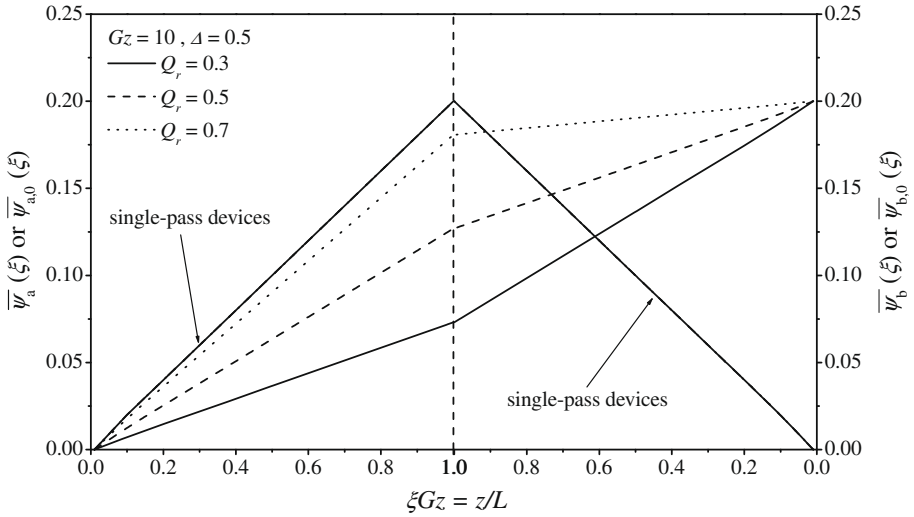

Fig. 7. Average fluid temperature distribution with Q_r as a parameter; $\Delta = 0.5$ and $Gz = 10$.

wall as shown in Fig. 6(b). Fig. 7 shows the fluid bulk temperature distribution along the fluid flowing direction. As indicated by Fig. 7, the bulk fluid temperature increases linearly along the fluid flowing direction, and the bulk fluid temperature distributions of single-pass devices for $Q_r = 0.3$, 0.5 and 0.7 are the same. The bulk exit temperature of the single-pass device equals to the double-pass one under the same Gz as shown in Fig. 7 due to the constant heat fluxes on the bottom and upper walls

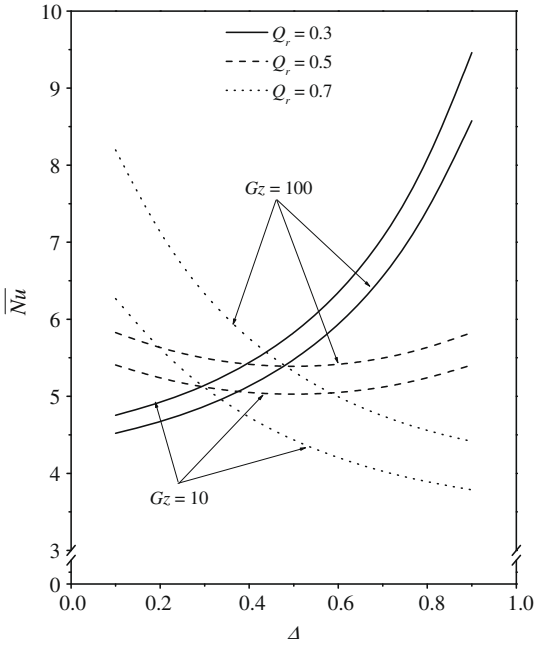

Fig. 8. Average Nusselt numbers vs. Δ with Q_r and Gz as parameters.

6.2. Heat-transfer efficiency enhancement and Power consumption increment

Nusselt number provides a measure of convection heat transfer occurring at the wall surface and usually is used to describe the heat-transfer efficiency in heat-transfer problems. The average Nusselt numbers with Gz, Δ and Q_r as parameters are illustrated in Fig. 8. As referred to Eq. (41), the $\overline{Nu}$ is inversely proportional to the average wall temperature $\overline{\psi}_s$, hence the larger $\overline{Nu}$ also implies that the lower average wall temperature will be obtained. As shown in Fig. 8, the $\overline{Nu}$ increases with increasing Gz. The influences of the impermeable-sheet location on $\overline{Nu}$ relate to Q_r and can be concluded three cases: (1) $Q_r = 0.3$: the $\overline{Nu}$ increases with increasing Δ; (2) $Q_r = 0.5$: the $\overline{Nu}$ increases as Δ moves away from 0.5; (3) $Q_r = 0.7$: the $\overline{Nu}$ increases with decreasing Δ. The comparison of average Nusselt numbers $\overline{Nu}_0$ and $\overline{Nu}$ and the corresponding heat-transfer efficiency enhancement I_h are shown in Table 2. The average Nusselt number of single-pass devices $\overline{Nu}_0$ increases with Gz but not varies with Q_r, as indicated in Table 2. Moreover, the heat-transfer efficiency enhancement I_h by employing a double-pass operation is defined in Eq. (43). As presented in Table 2, the double-pass devices perform better heat-transfer efficiency than that in single-pass devices, while the devices are operated in higher Gz. However, while low Gz is employed, say $Gz = 1$ as shown in

Table 3
The power consumption increment with impermeable-sheet location as a parameter.

I_P				
$\Delta = 0.1$	$\Delta = 0.3$	$\Delta = 0.5$	$\Delta = 0.7$	$\Delta = 0.9$
1000.37	38.95	15	38.95	1000.37

Table 2
The average Nusselt numbers $\overline{Nu}_0$ and $\overline{Nu}$ and I_h with Q_r as a parameter; $\Delta = 0.5$.

Gz	$\overline{Nu}_0$			$\overline{Nu}$			I_h(%)		
	$Q_r = 0.3$	$Q_r = 0.5$	$Q_r = 0.7$	$Q_r = 0.3$	$Q_r = 0.5$	$Q_r = 0.7$	$Q_r = 0.3$	$Q_r = 0.5$	$Q_r = 0.7$
1	4.12	4.12	4.12	0.79	0.65	0.56	−80.77	−84.15	−86.52
10	4.12	4.12	4.12	5.81	5.02	4.42	40.99	21.93	7.41
100	4.12	4.12	4.12	5.46	5.38	5.30	32.60	30.67	28.81
1000	4.12	4.12	4.12	5.39	5.38	5.38	30.96	30.77	30.58

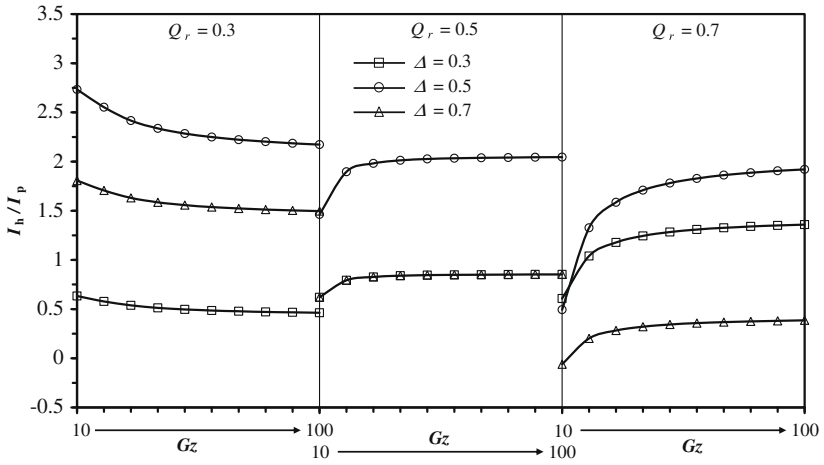

Fig. 9. The I_h/I_p with Δ as a parameter.

Table 2, the minus signs refer that the single-pass devices do better device performance than that in double-pass devices. The double-pass design increases the convective heat-transfer coefficient of fluid by increasing the average fluid velocity, however, the increment of the convective heat-transfer coefficient is insignificant for the case of lower Gz due to lower flowing rate. Hence, the performance of the single-pass devices is better than that in double-pass devices under lower Graetz number region, as shown in Table 2.

The double-pass operations not only enhance the heat transfer but also increase the power consumption simultaneously. The power consumption of a single-pass device is $P_0 = V\rho\ell w_{f,0} = 2.68 \times 10^{-7}$ J/s based on following working dimensions: $L = 1.2m$, $W = 0.04m$, $B = 0.2m$, $V = 1 \times 10^{-5}$ m^3/s, $\mu = 8.94 \times 10^{-4}$ kg/m s and $\rho = 997.08$ kg/m^3. As shown in Table 3, the power consumption increment I_p by employing double-pass devices increases with Δ moves away 0.5. Although the maximum power consumption of double-pass devices is 1000 times higher than that of single-pass devices for $\Delta = 0.1$ and 0.9, the corresponding power consumption is still small, say $P = 2.68 \times 10^{-4}$ J/s. Hence, it is reasonable to ignore the power consumption in all operation conditions.

As an economic sense, the consideration of both the heat-transfer efficiency enhancement I_h and the power consumption increment I_p is made in the form of I_h/I_p and the results are illustrated in Fig. 9. For three cases of $Q_r = 0.3$, 0.5 and 0.7, the highest values of I_h/I_p are obtained as $\Delta = 0.5$ due to the lowest power consumption increment, as shown in Fig. 9. The influences of $\Delta = 0.3$ and $\Delta = 0.7$ on I_h/I_p are different dependent on the values of Q_r. For $Q_r = 0.3$, the case of bottom wall with lower heat fluxes than upper wall, $\Delta = 0.7$ performs better I_h/I_p than $\Delta = 0.3$. For $Q_r = 0.5$, the symmetric heating case, the I_h/I_p of $\Delta = 0.7$ equals to $\Delta = 0.3$. Finally, for $Q_r = 0.7$, the case of bottom wall with higher heat fluxes than upper wall, $\Delta = 0.3$ has better I_h/I_p than $\Delta = 0.7$. Fig. 9 also indicates that the I_h/I_p increases with increasing Graetz numbers Gz for $Q_r = 0.5$ and 0.7 but decreases with increasing Graetz numbers Gz for $Q_r = 0.3$.

7. Conclusions

The heat-transfer phenomenon of double-pass parallel-plate heat exchangers with asymmetric wall heat fluxes and corresponding mathematical model were investigated and developed theoretically in this study. The analytical solutions for such conjugated Graetz problem were obtained by using the linear superposition of an asymptotic solution for the non-homogeneous part and an eigenfunction expansion in terms of power series for the homogeneous part. The effects of Graetz number Gz, impermeable-sheet location Δ and the wall heat flux ratio Q_r on the wall temperature, average fluid temperature distributions and the heat-transfer efficiency enhancement in a double-pass heat exchanger were discussed. The results show that the heat-transfer efficiency increases with increasing Gz. The influence of Δ on heat-transfer efficiency depends on the wall heat flux ratio Q_r and can be categorized to three cases. The heat-transfer efficiency increases with increasing Δ for the case of bottom wall with lower heat fluxes than upper wall, say $Q_r < 0.5$. For the case of bottom wall with higher heat fluxes than upper wall, say $Q_r > 0.5$, the heat-transfer efficiency increases with decreasing Δ. Furthermore, for the symmetric heating case, say $Q_r = 0.5$, the heat-transfer efficiency increases with Δ moves away from 0.5. The best selection of impermeable-sheet location by considering both heat-transfer efficiency enhancement and power consumption increment, say I_h/I_p, is $\Delta = 0.5$ as shown in Fig. 9. In conclusion, the double-pass design can readily improve the heat-transfer efficiency of a heat exchanger with asymmetric wall heat fluxes, comparing to the single-pass devices, and the present results can provide the selection guide of operating conditions to obtain the higher heat-transfer rate. The theoretical predictions of the wall temperature distribution of the double-pass devices are also helpful to choose the adequate materials to build up a heat exchanger with asymmetric heating.

Acknowledgement

The authors wish to thank the National Science Council of the Republic of China for its financial support.

References

[1] A. Laouadi, N. Galanis, C.T. Nguyen, Laminar fully developed mixed convection in inclined tubes uniform heated on their outer surface, Numer. Heat Transfer A 26 (1994) 719–738.
[2] R.K. Shah, A.L. London, Laminar Flow Forced Convection in Ducts, Academic Press, New York, 1995. pp. 196–207.
[3] R.D. Cess, E.C. Shaffer, Laminar heat transfer between parallel plates with an unsymmetrically prescribed heat flux at the walls, Appl. Sci. Res. Sec. A 9 (1959) 64–70.
[4] D.A. Nield, Force convection in a parallel plate channel with asymmetric heating, Int. J. Heat Mass Transfer 49 (2004) 5609–5612.
[5] J. Maletic, B. Mitrovic, B.S. Baclic, Some peculiarities of the asymmetric Graetz problem, Int. J. Eng. Sci. 44 (2006) 436–455.
[6] J.N.N., R. M. Cotta, Exact solutions for thermally developing tube flow with variable wall heat flux, Int. Commun. Heat Mass Transfer 21(5) (1994) 729–742.
[7] A. Barletta, E. Rossi di Schio, Effects of viscous dissipation on laminar forced convection with axially periodic wall heat flux, Heat Mass Transfer 35 (1999) 9–16.

[8] E. Papoutsakis, D. Ramkrishna, Conjugated Graetz problems. I: General formalism and a class of solid–fluid problems, Chem. Eng. Sci. 36 (1981) 1381–1390.
[9] E. Papoutsakis, D. Ramkrishna, Conjugated Graetz problems. II: Fluid–fluid problems, Chem. Eng. Sci. 36 (1981) 1393–1399.
[10] M.A. Bernier, B.R. Baliga, Conjugate conduction and laminar mixed convection in vertical pipes for upward flow and uniform wall heat flux, Numer. Heat Transfer A 21 (1992) 313–332.
[11] M.R. Amin, J.A. Khan, Effects of multiple obstructions on conjugate forced convection heat transfer in tube, Numer. Heat Transfer A 26 (1996) 265–279.
[12] X. Yin, H.H. Bau, The conjugated Greatz problem with axial conduction, Trans. ASME 118 (1996) 482–485.
[13] G.M. Brown, Heat or mass transfer in a fluid in laminar flow in a circular or flat conduit, AIChE J. 6 (1960) 179–183.
[14] R.J. Nunge, W.N. Gill, An analytical study of laminar counterflow double-pipe heat exchangers, AIChE J. 12 (1966) 279–289.
[15] H.M. Yeh, S.W. Tsai, C.L. Chiang, Recycle effects on heat and mass transfer through a parallel-plate channel, AIChE J. 33 (1987) 1743–1746.
[16] H.M. Yeh, C.D. Ho, The improvement of performance in parallel-plate heat exchangers by inserting in parallel an impermeable sheet for double-pass operations, Chem. Eng. Comm. 183 (2000) 39–48.
[17] C.D. Ho, H.M. Yeh, J.J. Guo, An analytical study on the enrichment of heavy water in the continuous thermal diffusion column with external refluxes, Sep. Sci. Technol. 37 (2002) 3129–3153.
[18] H.F. Zheng, X.S. Ge, Steady-state experimental study of a closed recycle solar still with enhanced falling film evaporation and regeneration, Renew. Energy 26 (2002) 295–308.
[19] M.H. Siegel, J.C. Merchuk, K. Schugerl, Air-lift reactor analysis: interrelationships between riser, downcomer, and gas–liquid separator behavior including gas recirculation effects, AIChE J. 32 (1986) 1585–1595.
[20] C.S. Bildea, A.C. Dimian, S.C. Cruz, P.D. Iedema, Design of tubular reactors in recycle systems, Comput. Chem. Eng. 28 (2004) 63–72.
[21] C.D. Ho, Y.J. Chuang, J.W. Tu, Double-pass flow heat transfer in a parallel-plate channel for improved device performance under uniform heat fluxes, Int. J. Heat Mass Transfer 50 (2007) 2208–2216.
[22] D.P.D. Incropera, Fundamentals of Heat and Mass Transfer, third ed., John & Sons, New York, 1990.